lajss.org© Latin American Journal of Solids and Structures
www.lajss.org

Analytical and Finite Element Modeling for Time-Dependent Deflection of Ultra-High-Performance Fiber-Reinforced Concrete Beam

Habibur Rahman Sobuz[a,h*], Ifran Shahriar Ayon[a], Noor Md. Sadiqul Hasan[b], Abdul Basit[c], Naimul Haque[d], Abdullah Alzlfawi[e], Tanvir Mustafy[f], Jihad Miah[g], Munir Hayet Khan[h]

[a]Department of Building Engineering and Construction Management, Khulna University of Engineering & Technology, Khulna - 9203, Bangladesh
[b]Department of Civil Engineering, International University of Business Agriculture and Technology, Dhaka 1230, Bangladesh. Email:
[c]Department of Civil Engineering, East West University, Dhaka 1212, Bangladesh
[e]Department of Civil and Environmental Engineering, College of Engineering, Majmaah University, Al Majmaah 11952, Saudi Arabia
[f]Department of Civil and Environmental Engineering, North South University, Dhaka 1229, Bangladesh
[g]Civil Engineering, School of Architecture, Technology and Engineering, University of Brighton, Lewes Road, Brighton BN2 4GJ, United Kingdom
[h]Faculty of Engineering & Quantity Surveying, INTI International University (INTI-IU), Persiaran Perdana BBN, Putra Nilai, Nilai 71800, Negeri Sembilan, Malaysia

*Corresponding author

Abstract

Ultra-high-performance fiber-reinforced concrete (UHPFRC) has emerged as an advanced concrete technology in the construction industry. It can provide better service in terms of strength, ductility, toughness, and stiffness than traditional concrete. This paper aims to analytically determine the time-dependent deflection (i.e., creep) of the UHPFRC beam with varying amounts of steel fiber addition. The age-adjusted effective modulus method was used to anticipate the time-dependent deflection of the UHPFRC beam. Experimental data related to time-dependent properties of UHPFRC were extracted from the literature to develop new formulas for creep coefficient and shrinkage strain through curve fitting and data validation. A new range of aging coefficient was proposed for UHPFRC through trial according to the ACI code. The existing shrinkage-induced curvature formula for cracked sections was modified using data validation. The analytical study incorporated all the proposed formulations and coefficient values to anticipate the UHPFRC beam's time-dependent deflection theoretically. Along with the analytic analysis, Finite Element Method (FEM) was also employed to predict the time-dependent deflection of the UHPFRC beam. It was found that for different percentages of steel fibers, both the FEM and the proposed analytical approaches conservatively estimate the deflection values, with an average deviation of around 20% from the experimental results. The accuracy and validation of the proposed theoretical formulation to predict the time-dependent deflection of UHPFRC beams were also demonstrated through statistical analysis.

Keywords
Ultra-High-Performance Concrete; Beam; Steel fiber; Time-dependent deflection; ANOVA; Sustained load

1 INTRODUCTION

Ultra-high-performance concrete (UHPC) is a new type of concrete that has significantly improved tensile and compressive strengths and enhanced durability (Rahman Sobuz et al., 2023; G. Yang et al., 2025; Zhu et al., 2020). UHPC is a cementitious composition made up of Portland cement, silica fume, fine silica sand, quartz flour, discontinuous internal steel or organic fibers, high-range water reducer, and a water-to-cement (W/C) ratio of less than 0.25 (Graybeal & Stone, 2012; Habibur Rahman Sobuz et al., 2024; Khan et al., 2023; Sobuz, Khan, et al., 2025; Sobuz, Rahman, et al., 2025). Mix design of UHPC is different from traditional concrete that incorporates the properties of High-Performance Concrete (HPC), Self-Consolidating Concrete (SCC), and Fiber Reinforced Concrete (FRC) (Akhnoukh & Buckhalter, 2021; Shi et al., 2025; Sobuz, Ahmed, Sutan, Sadiqul Hasan, et al., 2012; C. Yang et al., 2025; Zhang et al., 2024). Thus, UHPC can largely overcome traditional concrete's strength, ductility, toughness, and stiffness problems. UHPC poses high compressive and tensile strengths of 150 MPa and between 6.2 and 11.7 MPa, respectively (Resplendino, 2012). Besides, UHPC exhibits a higher flexural strength of about 48 MPa, depending on its material composition, design, and curing condition (Akid, Shah, et al., 2021; Huang et al., 2021; Perry & Zakariasen, 2004; Yao et al., 2022). Enhanced modulus of elasticity of UHPC ranging from 55-59 GPa contributes to the low deformation behavior at the elastic stage and early-age cracking (Akid, Wasiew, et al., 2021; Mishra, 2024; Russell et al., 2013). Optimized packing of fine and ultrafine particles and incorporation of steel fibers are responsible for the high compressive and ductile behavior of UHPC (Das et al., 2020; Kang et al., 2010; Liu et al., 2025; Sayed Mohammad Akid et al., 2023; Zhai et al., 2025). El-Din et al. (2016) used 1% to 3% steel fiber variation with aspect ratios of 30 and 50 to observe steel fiber effects on UHPC. The study found that compressive strength increased by 7.7% to 18.2% and flexural strength increased by 15% to 40% when steel fiber volume increased from 1% to 3%. The study also investigated compressive and flexural strength, which improved by 2% and 5% when the aspect ratio changed from 30 to 50. UHPFRC can provide a better solution for architectural and structural issues, but its practical implementation is mainly seen in bridge construction in several countries (Abbas et al., 2016; Ghasemi et al., 2023; Niu et al., 2024; Sun et al., 2017; Yao et al., 2025).

Time-dependent structural issues have become a significant concern for structural engineers and researchers in the last few decades. The beam is exposed to instantaneous and time-dependent deflections during the service period. Instantaneous deflection can be quantified immediately, which is not a critical issue; long-term time-dependent deflection can lead to severe structural problems over time. To this aim, several authors have proposed analytical modeling to conservatively predict time-dependent deflection. Most importantly, all these predictions were developed mainly focusing on the properties of standard strength concrete (NSC), and hence, time-dependent flexural analysis was also conducted due to the nonlinear effect of shrinkage and creep under sustained loading conditions (Hasan et al., 2019; Long et al., 2023; Sobuz, 2017; Sobuz, Kabbo, et al., 2025). Eventually, significant variations of deflections in the long run have been found due to its impact on the non-linear properties. The material composition and stress-strain relationship of UHPC and NSC are entirely different in existing literature (Ebadi Jamkhaneh & Kafi, 2018; Hasan et al., 2023; Miah et al., 2025; Sobuz et al., 2016; Yao et al., 2023). Besides, creep and shrinkage are two main attributes of time-dependent properties (Zhu et al., 2020). Ultimate creep coefficient and shrinkage strain for UHPC ranged from 0.1 to 0.32 and 45 to 800, respectively (Bărbos, 2016; Xu et al., 2018; Zhu et al., 2020). On the contrary, the ultimate creep coefficient and shrinkage strain for NSC ranged from 1.5 to 3 and were 726 micro-strains, respectively (Graybeal, 2006). In the case of NSC, it's observed that the creep coefficient increased or decreased proportionally with changes in service load over the long term (Bărbos, 2016; F. F. Al-Ajmai, 2018; Jabin et al., 2024). On the contrary, the creep behavior of UHPC is not significantly influenced by changes in service load (Flietstra et al., 2012; Hossain et al., 2023; Md. Sadiqul Hasan et al., 2015). Due to the different material properties of UHPC and NSC, it is impossible to generalize existing formulations for all types of concrete. Therefore, the analytical beam deflection approach of UHPC is still limited in the existing literature as no equation for UHPC has been developed. As the practical implementation of UHPC has increased several times compared to the past, it is crucial to develop a proper theoretical prediction for UHPC that can estimate time-dependent deflection within a reasonable margin of error. Furthermore, a well-developed study of beam deflection in UHPC can significantly reduce the time, cost, labor, and complexity of test setups.

In this paper, the time-dependent deflection of UHPFRC is predicted and compared with experimental data (Bărbos, 2016). Analytical prediction is developed by incorporating a proposed creep coefficient formula, a shrinkage strain formula, an aging coefficient value, and an assumed shrinkage-induced curvature formula into the existing analytical framework of the ACI Committee 435-R95 (2003). Experimental data are collected for varying percentages of steel fiber addition to analyze the effect of steel fiber on experimental deflection and analytical prediction. Finally, experimental results are compared with the analytical and FEM results to assess the accuracy of the prediction according to the updated framework of the ACI Committee 435-R95 (2003), and statistical analysis is also carried out.

2 Methodology

2.1 ACI committee 435-R95, 2003 Report

Age-adjusted effective modulus is a widely used numerical method for predicting stresses and deformations in structures subjected to creep (Khazanovich, 1990). ACI Committee 435R-95 (2003) reported the following formulations using the age-adjusted effective modulus method to theoretically predict the time-dependent deflection of cracked and uncracked concrete beam sections. Figure 1 represents an uncracked and cracked beam section.

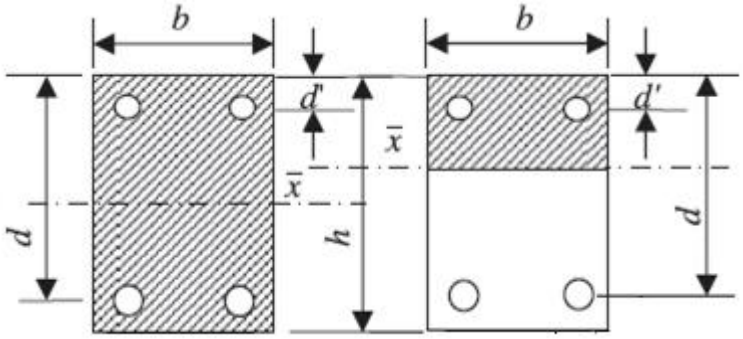

(a) (b)

Figure 1: (a) Un-cracked section and (b) Cracked section (Sobuz, Ahmed, Sutan, Hasan, et al., 2012)

The initial deflection of a supported beam can be evaluated using the following equation:

$$\Delta_{(t_0)} = \frac{5wl^4}{384E_cI_e} \quad (1)$$

Where, l = Effective span length, w = uniformly distributed load, E_c = Modulus of elasticity of concrete and I_e = Effective moment of inertia, which can be calculated from Branson's equation:

$$I_e = (\frac{M_{cr}}{M_a})^3 I_g + [1 - (\frac{M_{cr}}{M_a})^3] I_{cr} \leq I_g \quad (2)$$

Where, M_a = Maximum applied moment, I_g and I_{cr} = Moment of inertia of gross and cracked section, respectively.

$$I_{cr} = \frac{ba^3}{3} + nA_{st}(d-a)^2 + (n-1)A_{sc}(a-d')^2 \quad (3)$$

Where, b = Width of beam, a = Neutral axis depth for cracked section, $n = E_s / E_c$ = Modular ratio of steel to concrete, A_{st} and A_{sc} = Tensile and compression steel area, respectively, d = Effective depth of beam, d' = Depth of compression steel from top compression fiber, M_{cr} = Cracking moment, which is calculated using the following flexural formula:

$$M_{cr} = \frac{f_r I_g}{y_t} \quad (4)$$

Where f_r = Modulus of rupture of the concrete, y_t = Distance between the neutral axis and the tension face of the beam

ACI code provisions recommended creep and shrinkage formulations for analytical predictions in calculating the time-dependent deflection. Hence, the following formulation evaluates the creep coefficient at time *t* (days) after load application.

$$C_t = C_U \frac{t^{0.6}}{10 + t^{0.6}} \quad (5)$$

Where, C_u = Ultimate creep coefficient, which depends on the condition of the concrete. On average, a value of 1.6 is used.

Age-adjusted effective modulus can be determined using the following formulation:

$$E_{c.t} = \frac{E_c(t_0)}{1+\lambda C_t} \quad (6)$$

$E_c(t_0)$ = Modulus of elasticity of concrete at initial period, λ = Aging coefficient, which varies between 0.7 to 0.9 with an average value of 0.8

Using transformed section analysis, neutral axis depth can be computed at any time following the age-adjusted effective modulus method. After *t* period of load application, the $I_{cr.t}$ (moment of inertia of the cracked section) and $I_{e.t}$ The effective moment of inertia (EMI) of the cracked section can be determined using the neutral axis depth. Finally, deflection due to the creep effect can be calculated by substituting in equation (1).

Shrinkage deflection can be determined by following the recommended model of the ACI code. The following expression can be used to calculate the shrinkage strain at any time *t*:

$$\varepsilon_{sh(t)} = \varepsilon_{sh.u}\frac{t}{a+t} \quad (7)$$

Where, $\varepsilon_{sh.u}$ = Ultimate shrinkage strain, which differs from 800×10^{-6}, a = Empirical constant, with values of 35 for moist-cured concrete and 55 for steam-cured concrete, respectively.

The Shrinkage-induced curvature of a reinforced concrete section can be determined using the following expression(Gilbert, 2001):

$$k_{sh} = \frac{k_r\varepsilon_{sh(t)}}{D} \quad (8)$$

Where, D = Total depth of the section, k_r = Factor depends on the amount and placement of the bonded reinforcement. For a cracked reinforced concrete section subjected to pure bending, the value of K_r is given by:

$$k_r = 1.2\left[1-0.5\frac{A_{sc}}{A_{st}}\right]\left(\frac{D}{d}\right) \quad (9)$$

Whereas, for the un-cracked section, the factor K_r is given by:

$$k_r = (1000\rho - 2500\rho^2)\left(\frac{d}{0.5D}-1\right)\left(1-\frac{A_{sc}}{A_{st}}\right)^{1.3} \text{ when the steel ratio, } \rho = \frac{A_{st}}{bd} \le 0.01 \quad (10)$$

$$\text{Or, } k_r = (40\rho + 0.35)\left(\frac{d}{0.5D}-1\right)\left(1-\frac{A_{sc}}{A_{st}}\right)^{1.3} \text{ when the steel ratio, } \rho = \frac{A_{st}}{bd} > 0.01 \quad (11)$$

For a supported beam, the deflection due to shrinkage can be expressed as:

$$\Delta_{(sh)} = \frac{1}{8}k_{sh}l^2 \quad (12)$$

Finally, shrinkage deflection is added with previously determined "deflection due to creep effect" to determine the total time-dependent deflection.

2.2 Creep Coefficient

The ACI Committee's proposed equation generates a much higher creep coefficient value for UHPFRC beams than experimental data. This study suggests the following formula, which is based on the equation of (Zhu et al., 2020).

$$C_t = C_u\sqrt{\frac{t}{a+t}} \quad (13)$$

This equation was developed through data validation and curve fitting with experimental data and the graph of Bărbos (2016). The ultimate creep coefficient C_U was assumed to be 0.1 - 0.32, according to (Ahmed & Sobuz, 2011a; Bărbos, 2016). Here, the curve fitting factor is 0.5, where empirical constant *a* = 35 for 0% steel fiber and 15 for all other steel fiber variations. Hence, Figure 2 depicts the analytical and experimental creep coefficient values varying the steel fiber percentages.

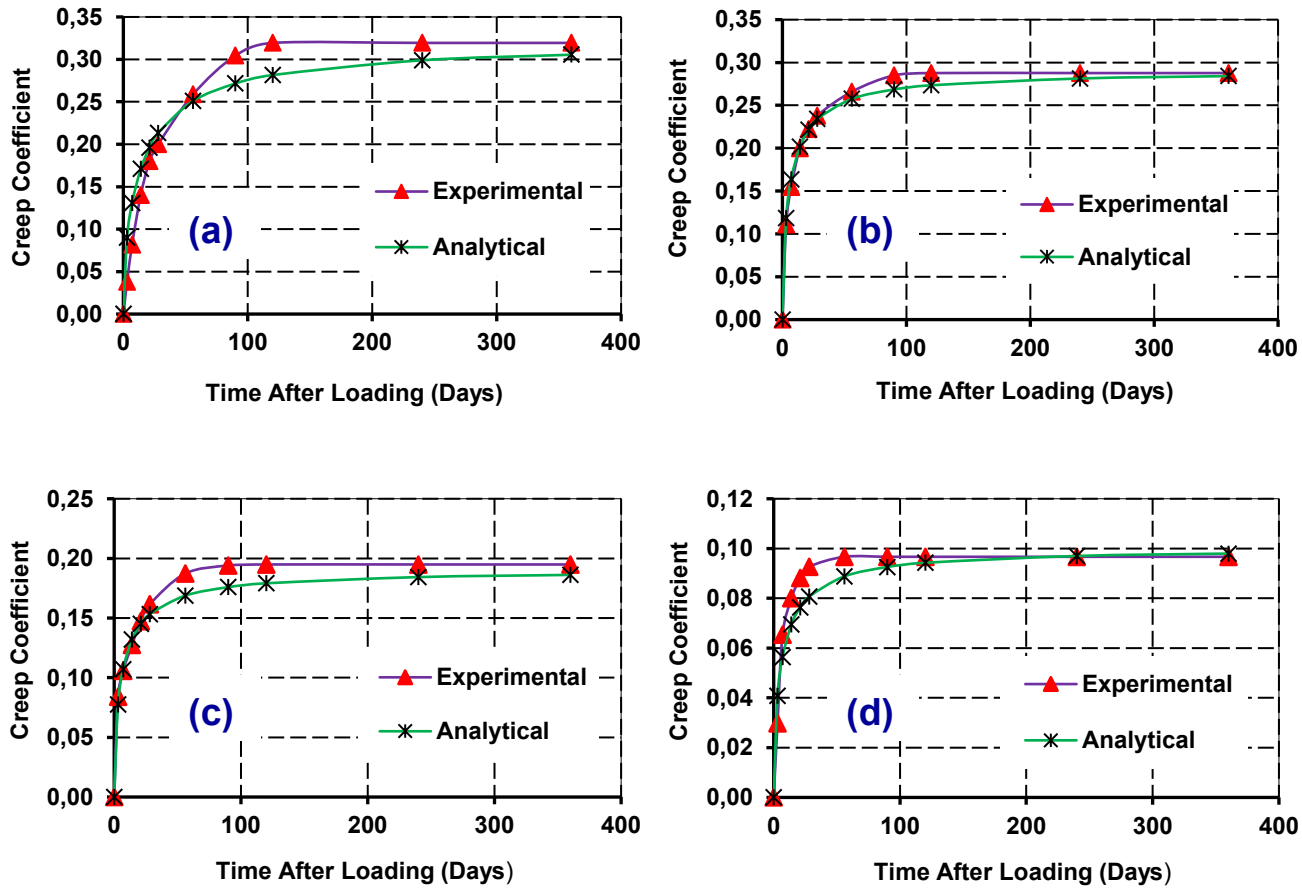

Figure 2: Analytical and experimental creep coefficient: (a) 0% steel fiber, (b) 0.5% steel fiber, (c) 1.5% steel fiber, and (d) 2.55% steel fiber.

2.3 Shrinkage Strain

The ACI Committee's proposed equation generates a much higher shrinkage strain value for the UHPFRC beam than the experimental data. This study suggests the following equation, which is based on the equation of (Zhu et al., 2020).

$$\varepsilon_{sh(t)} = \varepsilon_{sh.u}\sqrt{\frac{t}{b+t}} \tag{14}$$

This equation is developed through data validation and curve fitting with (Wu et al., 2019) and (Graybeal, 2006) extracted experimental data and graph analyses. Ultimate shrinkage strain is assumed to vary between 45×10^{-6} to 830×10^{-6}according to Yoo et al. (2018), Ahmed and Sobuz (2011b), Sobuz et al. (2011) and Wu et al. (2019). Here, the curve fitting factor is 0.5. Empirical constant *b* is 10 for any percentage of steel fiber addition. Hence, Figure 3 represents the analytical and experimental shrinkage strain with variations in steel fiber percentages.

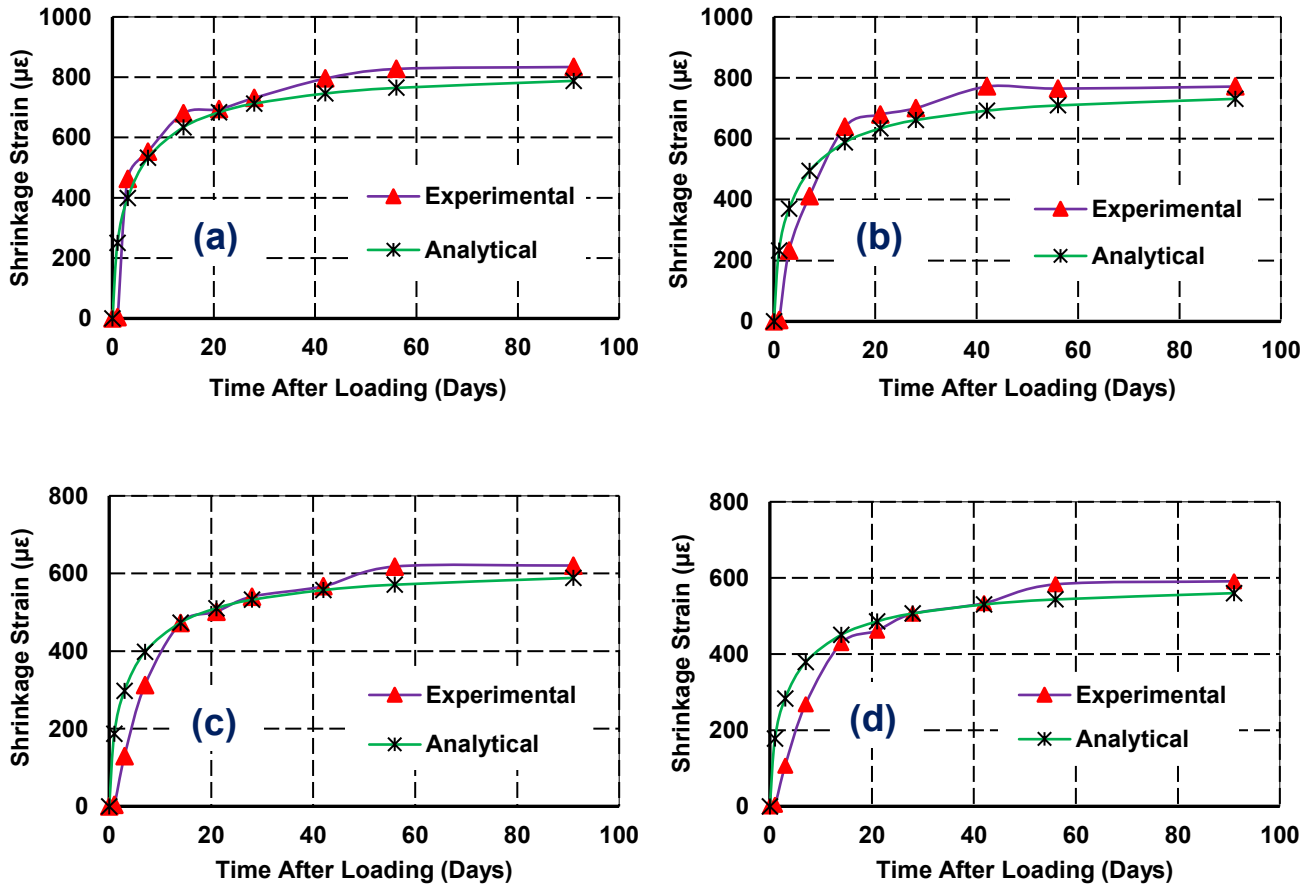

Figure 3: Analytical and experimental shrinkage strain: (a) 0% steel fiber, (b) 1% steel fiber, (c) 2% steel fiber, and (d) 3% steel fiber

2.4 Aging Coefficient

Another critical factor is the aging coefficient, which depends on concrete properties. According to the ACI code, this value can vary from 0 to 1, but in most cases, it's used between 0.7 and 0.9. Zvolánek and Terzijski (2017) reported that the aging coefficient value for High Strength Concrete (HSC) is 0.45. It's observed that the aging coefficient decreases with the increase in stiffness value. UHPC is stiffer than HSC, so its aging coefficient should be lower than 0.45. This study proposes a new aging coefficient value through several trials following the ACI code. Hence, it is observed that a value between 0.1 and 0.5 provides a conservative estimation of experimental results. However, on average, it can be used as much as 0.3.

2.5 Shrinkage Induced Curvature

The shrinkage-induced curvature formulas defined by (Gilbert, 2001) and (Branson, 1977) overestimate the shrinkage deflection of the cracked UHPFRC beam section. After trialing several formulations, it was found that shrinkage deflection can be calculated within an acceptable limit when the factor defined by Kilpatrick and Gilbert (2018) is incorporated into the formulation reported by (Gilbert, 2001). Therefore, the proposed equation for the cracked section of the UHPFRC beam is as follows:

$$k_r = 1.2\left(\frac{I_{cr}}{I_e}\right)^{0.67}\left[1 - 0.5\frac{A_{sc}}{A_{st}}\right]\left(\frac{D}{d}\right) \quad (15)$$

Equation (9) is replaced by equation (15) to determine the shrinkage deflection of a cracked section of the UHPFRC beam.

2.6 Input value

Four beams are considered here for the analytical prediction of long-term deflection. This study's UHPFRC beams with 0%, 0.5%, 1.55%, and 2.55% steel fiber addition are denoted as CB 0, SB 0.5, SB 1.5, and SB 2.55, respectively. Simply supported I beam with a dimension of 120 mm x 240 mm x 3200 mm is taken for all the steel fiber ratios. Analytical long-term deflection is calculated for different sustained load and steel fiber ratios to explore their effect. Sustained loads level for analytical prediction is shown in Table 1. The service load is the ultimate flexural capacity multiplied by 0.2, 0.25, and 0.31 factors. These factors are based on the first cracking load, and the usual loads are more significant than the first cracking load that any member experiences under service conditions. The ultimate flexural capacity of all four beams is calculated using the equivalent rectangular stress block of the beam's cross-section in accordance with the BS 8110-1 (1997) code of practice (E. Ahmed, & Sobuz, H. R. , 2011; E. Ahmed, Sobuz, H. R., & Sutan, N. M., 2011; Sobuz & Ahmed, 2011; Sobuz et al., 2023). Finally, analytical deflections are compared with the previous experimental results of different authors. Loading of the beam for a long-term deflection test is shown in Figure 4.

Table 1 Sustained Load Level

Total Sustained Load P_s (kN)	Steel Fiber Volume							
	0%		0.5%		1.5%		2.55%	
	Beam	P_s / P_0^a	Beam	P_s / P_1^b	Beam	P_s / P_2^c	Beam	P_s / P_3^d
17.5	CB 0-20	0.2	SB 0.5-20	0.2	SB 1.5-20	0.20	SB 2.55-20	0.2
21.5	CB 0-25	0.25	SB 0.5-25	0.25	SB 1.5-25	0.25	SB 2.55-25	0.25
26.5	CB 0-31	0.31	SB 0.5-31	0.31	SB 1.5-31	0.31	SB 2.55-31	0.31

Note: CB 0–20 indicates control beam with 0% steel fiber subjected to 20% of its ultimate flexural capacity, SB 0.5-20 indicates steel fiber beam with 0.5% steel fiber subjected to 20% of its ultimate flexural capacity (All other notations follow a similar pattern).

P_0^a : Flexural capacity of CB 0 (ρ_{SF} of 0%) = 85.7 kN

P_1^b : Flexural capacity of SB 0.5 (ρ_{SF} of 0.5%) = 85.8 kN

P_2^b : Flexural capacity of SB 1.5 (ρ_{SF} of 1.5%) = 86.0 kN

P_3^c : Flexural capacity of SB 2.55 (ρ_{SF} of 2.55%) = 86.2 kN

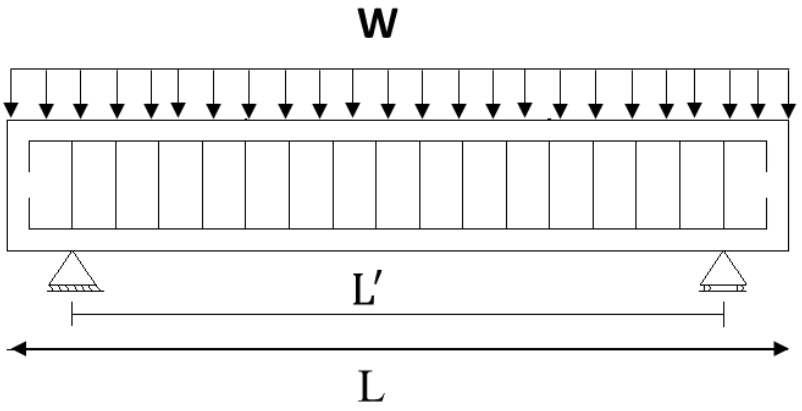

Figure 4: Loading of beam for long-term deflection test.

3 Results and Discussions

3.1 Effect of Sustained Load Level

Figure 5 shows the creep coefficient (ratio of time-dependent deflection to instantaneous deflection) for different sustained load levels. The time vs. ratio curve shows linear behavior for CB 0 and SB 0.5 at initial periods. After 28 days, the increase in ratios with time is negligible. On the other hand, for SB 1.5 and SB 2.55, no significant increment was observed with time after the development of initial deflection. It has been observed that the ratio decreases when the sustained load level increases. According to Tan and Saha (2006), when sustained load increases in a beam section, a significant increase in instantaneous deflection occurs compared to the time-dependent deflection. That's why the ratio decreases with the increased level of sustained load. This same material behavior is also visible in the present analytical investigation. For CB 0 and SB 0.5, it's found that the difference between the ratios of time-dependent to instantaneous deflection for different sustained loads maintain almost similar values up to 28 days and then differentiated by different percentages up to the stabilization period. However, in the case of SF 1.5 and SF 2.55, the ratios for varying sustained loads are nearly similar from 3 days until the stabilization period.

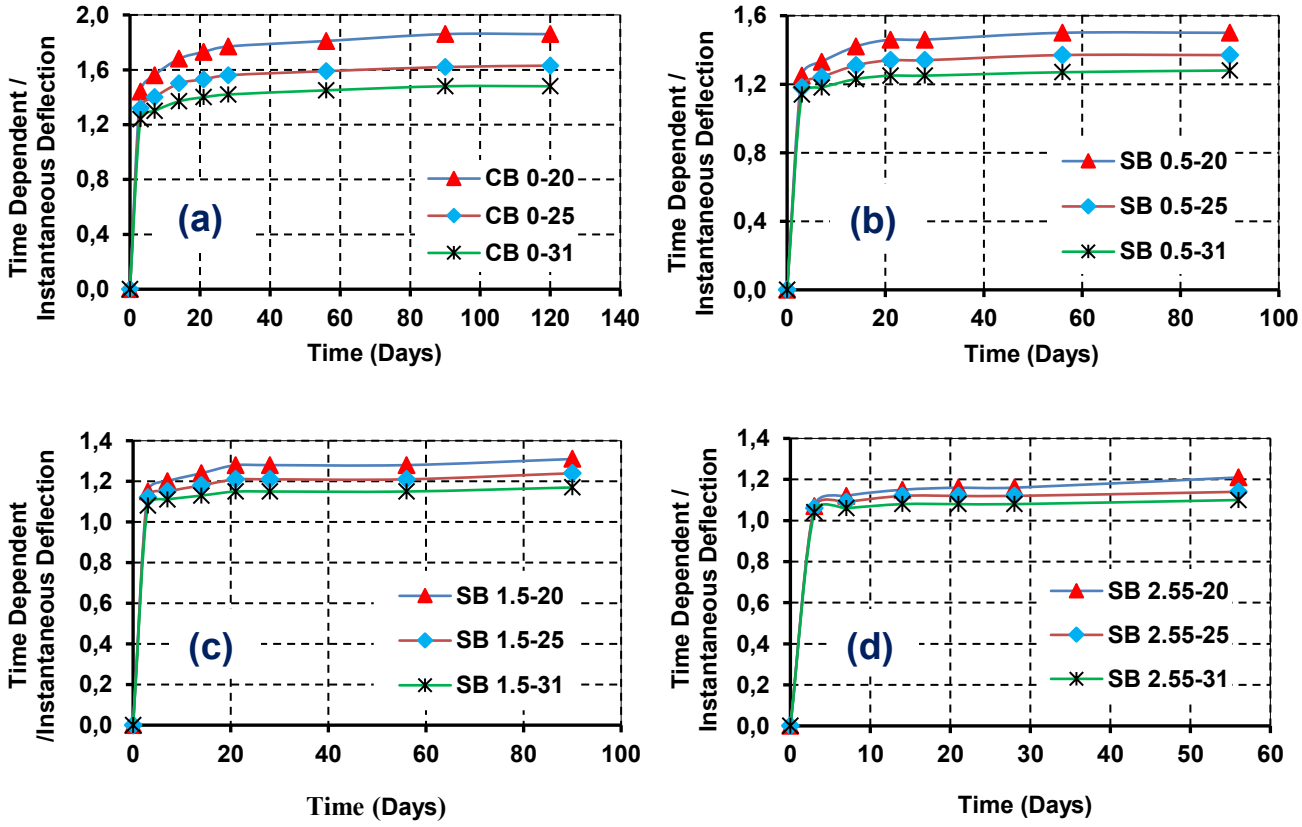

Figure 5: Comparison of mid-span deflection under different sustained loads (a) 0% SF, (b) 0.5% SF, (c) 1.5% SF, and (d) 2.55% SF.

3.2 Effect of Steel Fiber

Figures 6-8 represent a comparison of beam total deflection, time-dependent deflection, and creep coefficient for different steel fiber ratios under the same sustained load. For all the steel fiber ratios, the initial slope of the time-deflection curve shows a linear relationship up to 28 days. After 28 days, the increase in deflection with time is relatively insignificant up to the stabilization period of the beam (Chen et al., 2024). In contrast, the control beam shows linear relationships between time and deflection throughout the entire service period of the beam. Under the sustained load of the control beam (0.2 P_0^a), the time-dependent deflections of SB 0.5-20, SB 1.5-20, and SB 2.55-20 are 21%, 32%, and 40% less, respectively, compared to the control beam (CB 0-20) at the stabilization period. Under the sustained load of the control beam (0.25 P_0^a), the time-dependent deflection of SB 0.5-25, SB 1.5-25, and SB 2.55-25 were 18%, 26%, and

24% less, respectively, compared to the control beam (CB 0-25). When the sustained load is increased to the service load of the control beam (0.31 P_0^a), SB 0.5-31, SB 1.5-31, and SB 2.55-31 exhibit 14%, 22%, and 28% less, respectively, time-dependent deflection compared to the control beam (CB 0-31). According to (Bărbos, 2016), the time-dependent deflection of SB 0.5, SB 1.5, and SB 2.55 were 22%, 34%, and 44% less compared to the control beam (CB-0). Therefore, from experimental data, the deflection deviation of steel fiber beams increased while the time-dependent deflection decreased with the increment of steel fiber content. This phenomenon is also noticeable in the analytical predictions for different sustained load levels.

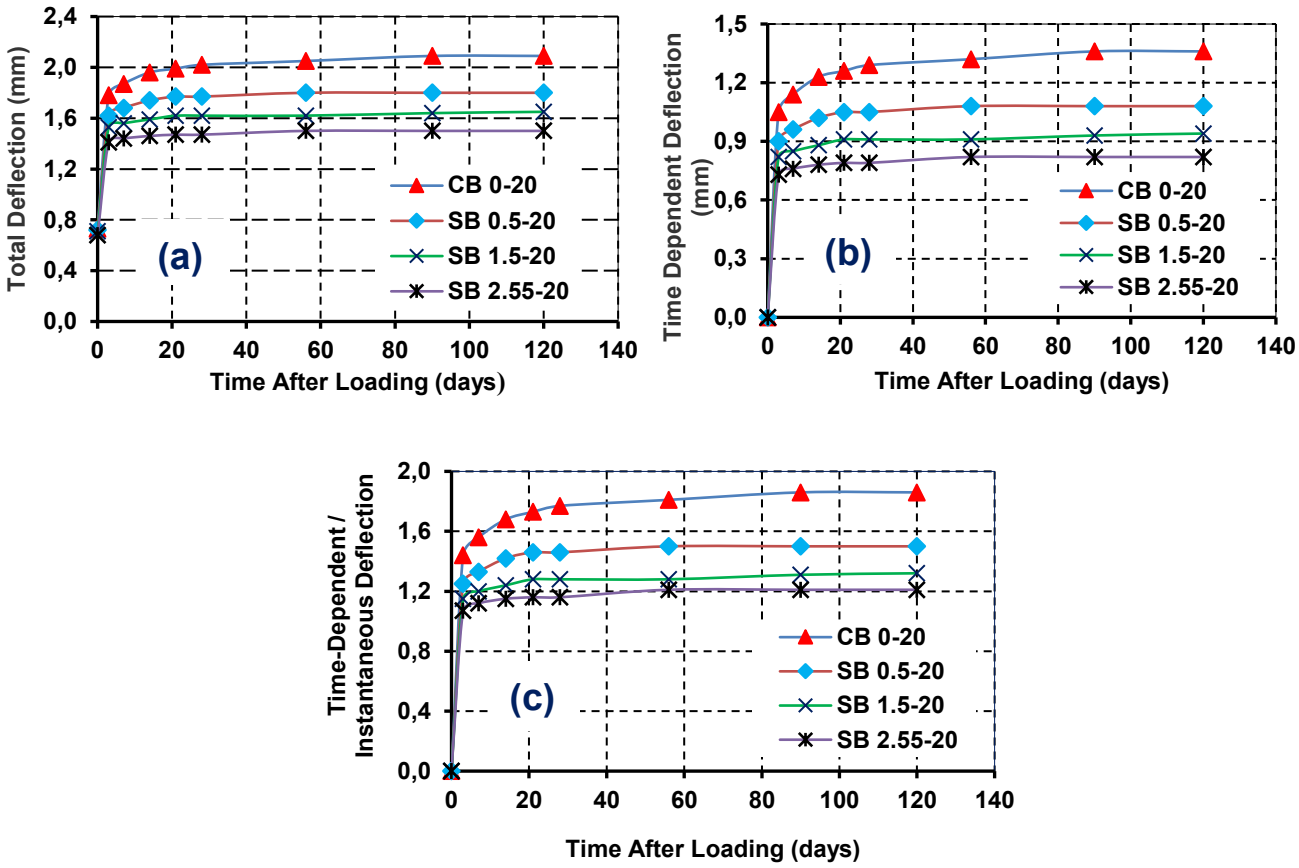

Figure 6: UHPFRC beam with different steel fiber ratios subjected to a service load 0.2*p* : (a) total deflection, (b) time-dependent deflection, and (c) ratios of time-dependent to instantaneous deflection.

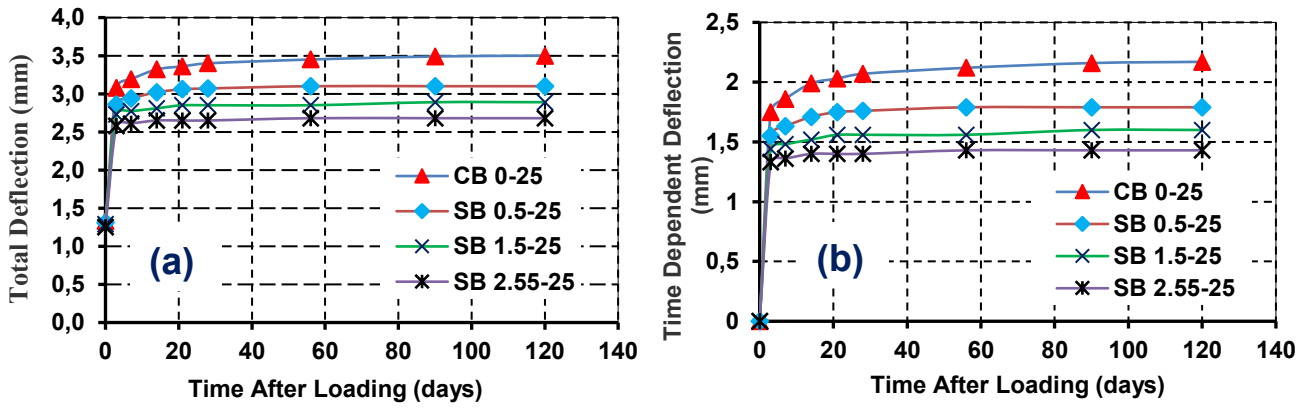

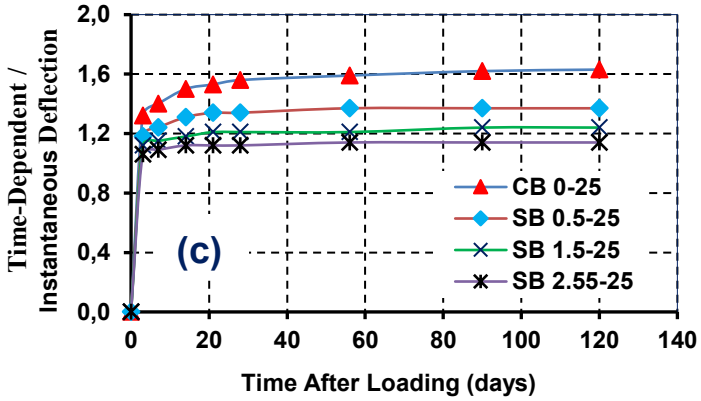

Figure 7: UHPFRC beam with different steel fiber ratios subjected to a service load 0.25*p*: (a) total deflection, (b) time-dependent deflection, and (c) ratios of time-dependent to instantaneous deflection

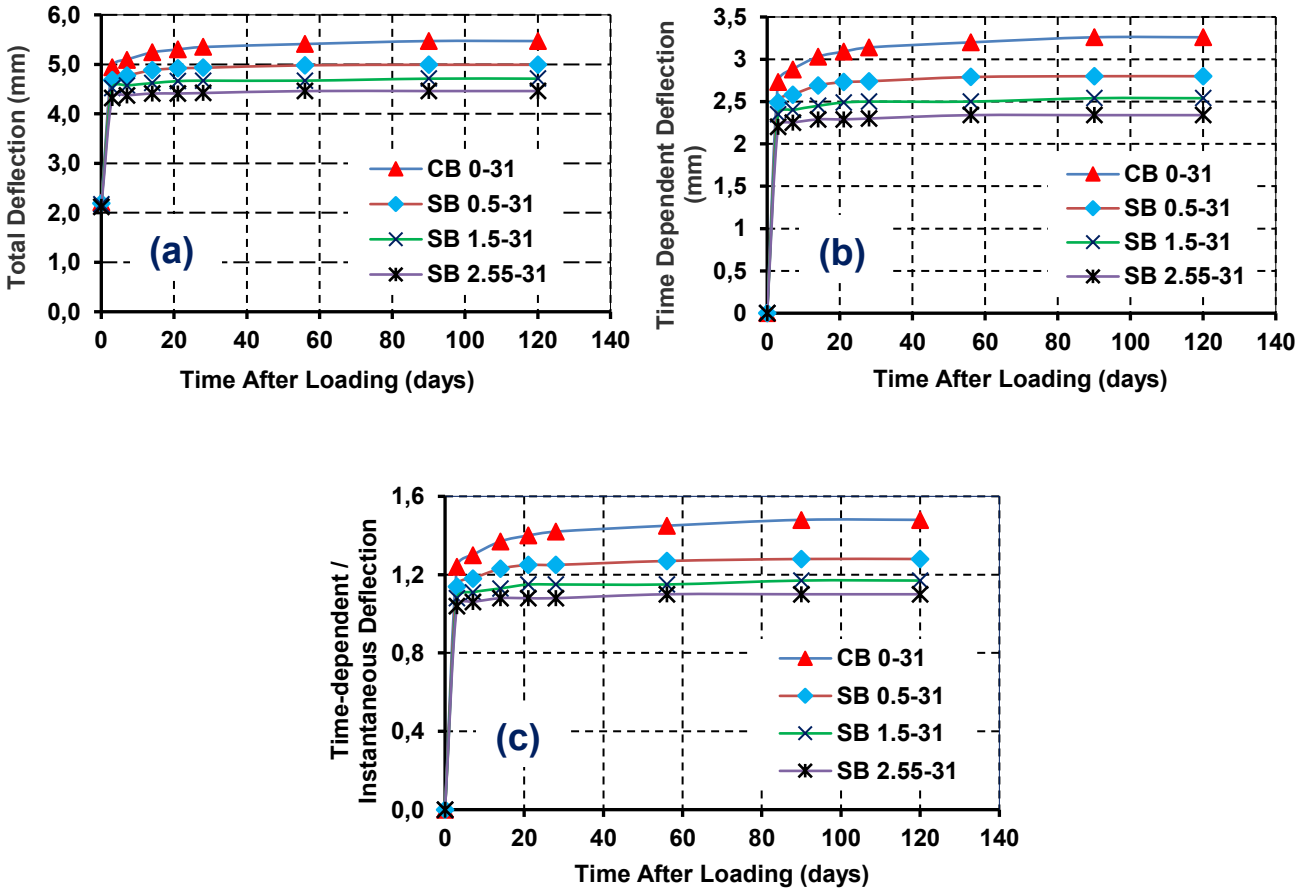

Figure 8: UHPFRC beam with different steel fiber ratios subjected to a service load 0.31*p*: (a) total deflection, (b) time-dependent deflection, and (c) ratios of time-dependent to instantaneous deflection.

3.3 Statistical analysis

Regression and ANOVA results for UHPFRC beam with different steel fiber ratios subjected to varying levels of service load of 17.5 kN, 21.5 kN, and 26.5 kN such as (a) total deflection (b) time-dependent deflection (c) ratios of time-dependent to instantaneous deflection were carried out, and the results are shown in Table 2. The extraordinarily high values of R^2 and adjusted R^2 (≥ 0.9996) across all load cases indicate near-perfect correlation and model fit, validating

the robustness of the regression model. The low standard error further supports the precision of the predictions (Mishra et al., 2025). ANOVA results reveal extremely significant F-values (greater than 60,000 in all cases) with corresponding p-values well below 0.05, affirming the statistical significance of the model parameters. The coefficients for time-dependent deflection and its ratio to instantaneous deflection suggest a strong dependence of the overall deflection behavior on time-dependent effects, particularly under higher loads. This highlights the importance of incorporating time-dependent parameters in analyzing UHPFRC beams under sustained loading conditions, ensuring accurate long-term performance predictions. These findings provide critical insights into the behavior of UHPFRC beams, informing both theoretical understanding and practical applications.

Table 2 Regression and ANOVA results for UHPFRC beam with different steel fiber ratios subjected to varying levels of service load (a) total deflection, (b) time-dependent deflection, and (c) ratios of time-dependent to instantaneous deflection.

	17.5 kN			**21.5 kN**			**26.5 kN**		
Multiple R	0.9998			0.9998			0.9999		
R^2	0.9997			0.9997			0.9998		
Adjusted R^2	0.9997			0.9996			0.9998		
Std Error	0.0064			0.0106			0.0118		
Total	44			44			44		
DF	2								
ANOVA	F-Value		Sign. F	F-Value		Sign. F	F-Value		Sign. F
	65507		1.42E-72	60704		6.80E-72	109700		3.67E-73
Regression	Coeff.	Standard Error	P-value	Coeff.	Standard Error	P-value	Coeff.	Standard Error	P-value
Intercept	1.1	1.28	2.21E-65	1.2966	0.0052	9.3E-67	2.1733	0.0058	5.6E-74
Time-Dependent Deflection	1.57	1.2	2.25E-34	1.7910	0.0487	5E-33	1.8950	0.0532	1.8E-32
Time-Dependent / Instantaneous Deflection	25.02	6.25	2.00E-19	-1.0286	0.0649	4.3E-19	-1.9474	0.1172	8.2E-20

3.4 Numerical Modeling

In this study, a three-dimensional nonlinear finite element model (FEM) of a UHPFRC beam was developed using commercial finite element software, ABAQUS/CAE, to simulate the structural response of UHPFRC beams under applied loads. The model was crafted to capture the complex interaction between concrete and steel reinforcement and the material nonlinearities inherent to UHPFRC under loading conditions. The following subsections detail the modeling techniques, including geometric configuration, material definitions, boundary conditions, loading protocols, solution algorithms, and failure analysis.

Geometric modeling

The geometry of the FRC beam was discretized using eight-node linear brick elements (C3D8R) with reduced integration. This choice minimizes computational costs and mitigates shear locking and hour-glassing effects, both common challenges in the nonlinear analysis of concrete structures. The mesh size was set to 10 mm by 10 mm, following a comprehensive mesh sensitivity analysis to balance computational efficiency with the accuracy needed to capture stress concentration and crack propagation. Two-node linear truss elements (T3D2) were embedded within the concrete volume for the steel reinforcement. Truss elements were chosen for their simplicity and efficiency in modeling axial load-bearing capacity without capturing bending effects, as the primary reinforcement behavior in concrete is axial under flexural loading. The ABAQUS embedded region constraint was applied, with the concrete beam defined as the host region and the steel bars as the embedded region. This constraint enabled nodes in the reinforcement elements to

conform to the deformation of the surrounding concrete, ensuring load transfer and eliminating the need for complex contact interactions between concrete and steel. Figure 9 shows the reinforcement detailing within the beam.

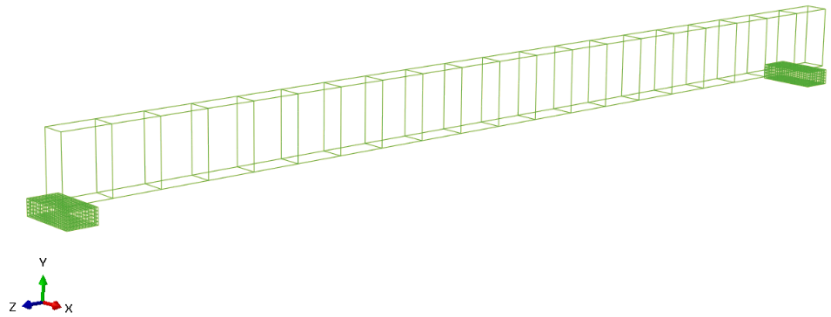

Figure 9: Reinforcement detailing of the model

In this model, the interaction between concrete and steel reinforcement was simulated using the embedded region constraint available in ABAQUS, which assumes a perfect bond between the two materials. This constraint ensures that the reinforcement nodes follow the deformation of the surrounding concrete mesh. While this assumption simplifies the modeling process by neglecting bond-slip behavior, it is justified in this study as UHPFRC exhibits a dense microstructure and high matrix integrity due to fiber bridging, which greatly limits slip at the interface. However, it is acknowledged that this modeling approach may not fully capture local stress concentrations or debonding effects at the steel-concrete interface under extreme loading conditions.

Material modeling

The concrete in this model was characterized using ABAQUS's Concrete Damaged Plasticity (CDP) model, specifically chosen to capture both the tensile cracking and compressive crushing behaviors that characterize UHPFRC under load. The CDP model's key parameters-dilation angle, flow potential eccentricity, biaxial/uniaxial stress ratio, and yield stress ratios-were calibrated based on experimental data to match the nonlinear behavior observed in the material. This calibration process defined the uniaxial stress-strain response curves to represent UHPFRC's distinctive post-cracking degradation and tension-stiffening effects. This ensured the model could accurately simulate concrete strain softening, tension stiffening, and compressive damage accumulation. An elastoplastic material model with isotropic hardening was used for the steel reinforcement to simulate yielding and subsequent strain-hardening. The mechanical properties, such as yield strength, Young's modulus, and strain-hardening modulus, were specified according to the experimental test data for the reinforcing steel. This approach allowed the model to effectively simulate stress redistribution between the concrete matrix and steel reinforcement, particularly under load reversals and plastic deformation states. Additionally, sustained load effects and the influence of varying steel fiber ratios were modeled to examine long-term deflection behaviors, with adjustments made to capture the creep and relaxation responses as influenced by fiber content. Table 3 summarizes the key parameters adopted in the ABAQUS simulation for both UHPFRC and reinforcing steel, including mechanical properties and CDP-specific inputs. These values were chosen based on literature, ABAQUS documentation, and convergence studies to ensure numerical stability and physical fidelity.

Table 3. Parameters used in finite element simulation

PARAMETER	VALUE	REFERENCE/NOTE
ELASTIC MODULUS OF UHPFRC (E_c)	55,000 MPa	Based on literature (Graybeal & Stone, 2012)
POISSON'S RATIO OF UHPFRC (N)	0.18	Typical for UHPFRC
COMPRESSIVE STRENGTH (f'_c)	150 MPa	Experimental/literature (Zhu et al., 2020)
TENSILE STRENGTH (f_t)	10 MPa	Estimated for UHPFRC
DILATION ANGLE (Ψ)	36°	Recommended for CDP (ABAQUS manual)
FLOW POTENTIAL ECCENTRICITY (E)	0.1	Recommended for CDP
RATIO OF BIAXIAL TO UNIAXIAL COMPRESSIVE STRENGTH (F_{B0}/F_{C0})	1.16	Default value in CDP model

KC (SECOND STRESS INVARIANT RATIO)	0.667	Default value in CDP model
VISCOSITY PARAMETER (M)	0.0001	Default for numerical stability
ELASTIC MODULUS OF STEEL (E_S)	200,000 MPa	Standard for reinforcement steel
YIELD STRENGTH OF STEEL ($\boldsymbol{\sigma_y}$)	500 MPa	Based on test data
HARDENING MODULUS OF STEEL ($\boldsymbol{E_h}$)	2,000 MPa	Estimated for post-yield behavior

To represent the nonlinear behavior of ultra-high-performance fiber-reinforced concrete (UHPFRC), the Concrete Damaged Plasticity (CDP) model was used in ABAQUS. This model simulates both tensile cracking and compressive crushing through damage accumulation. The flow potential function is given by:

$$G = \sqrt{(\varepsilon \cdot \tan\psi)^2 + q^2} - p \cdot \tan\psi \quad (16)$$

where ψ is the dilation angle, ε is the flow potential eccentricity, q is the Mises equivalent effective stress, and p is the hydrostatic pressure. The yield function is defined as:

$$F = \frac{1}{1-\alpha}(q - 3\alpha p) + \beta\langle\sigma_{max}\rangle - \sigma_c \quad (17)$$

where α is the ratio of biaxial to uniaxial compressive strength, β is a material constant, σ_{max} is the maximum principal stress, and σ_c is the uniaxial compressive strength. For steel reinforcement, an elasto-plastic model with isotropic hardening was used. The stress-strain relationship is expressed as:

Elastic region:

$$\sigma = E \cdot \varepsilon \quad for \quad \varepsilon \leq \varepsilon_y \quad (18)$$

Plastic region:

$$\sigma = \sigma_y + E_h(\varepsilon - \varepsilon_y) \quad for \quad \varepsilon > \varepsilon_y \quad (19)$$

where E is Young's modulus, σ_y is the yield stress, E_h is the hardening modulus, and ε_y is the yield strain. These models are calibrated using literature values and validated to capture the nonlinear response of UHPFRC under service and flexural loading.

Boundary conditions and loading

Appropriate boundary conditions were applied to replicate a supported beam scenario: one end of the beam was pinned, restricting all translational degrees of freedom in the y and z directions, while the other end was assigned a roller boundary condition, constrained only in the y-direction. This configuration replicates real-world support conditions and allows for free expansion or contraction along the beam's length, capturing realistic load distribution and support reactions. A four-point bending setup was implemented, replicating experimental loading conditions by applying two concentrated loads as pressure over specified areas. These loads were defined in the Static, General step, incrementally applied to simulate a gradual increase in load and capture both elastic and plastic responses in the concrete and steel. Load increments were applied smoothly to minimize potential dynamic effects and allow accurate cracking and crushing initiation simulation. Additionally, ABAQUS's load control was set up to monitor strain rates, helping to stabilize the simulation during high nonlinear response stages.

Solution Algorithm

The model's solution strategy relied on ABAQUS's nonlinear static analysis capabilities, which were employed to handle complex material behavior, large deformations, and load-induced damage progression. The Static, general step was configured with an incremental-iterative approach that utilized an automatic stabilization factor to maintain

numerical stability during phases of high nonlinearity, such as cracking or crushing in the concrete. The initial arc length increment was specified at 0.01 to control load progression smoothly, while minimum and maximum increments were set at 1×10E5 and 1, respectively, to optimize convergence without excessive computation time. The Newton-Raphson method was selected as the primary solver for convergence, allowing iterative adjustment of the load increments based on ABAQUS's convergence criteria. To accommodate high strain zones and nonlinear material response, ABAQUS's adaptive meshing and automatic step size control were enabled, ensuring the model could adapt increment sizes as required to reach convergence within acceptable tolerance limits.

Numerical failure mode

The model's failure mode was examined through stress and strain contours generated in ABAQUS, allowing a detailed assessment of failure mechanisms. Figure 10 plots the Logarithmic strain contours, highlighting areas with high deformation and showing critical zones likely to experience failure. Von Mises stress contours illustrated stress distribution within the concrete matrix and provided insights into load transfer and stress accumulation, as displayed in Figure 11. Additionally, stresses within the reinforcement were evaluated to assess the interaction between steel and concrete, plotted in Figure 12. The results demonstrated load-sharing behavior between the concrete and steel, with fiber reinforcement contributing to increased tensile capacity. Contour plots generated in ABAQUS allowed for a visual assessment of localized stresses and strains, aiding in understanding failure progression. The progression of deformation is illustrated in Figure 13, corresponding to 50% and 100% of the applied load, respectively. At 50% loading, the beam exhibits elastic curvature with pronounced mid-span deflection, while at 100% load, significant flexural deformation and failure patterns are evident, consistent with experimental observations.

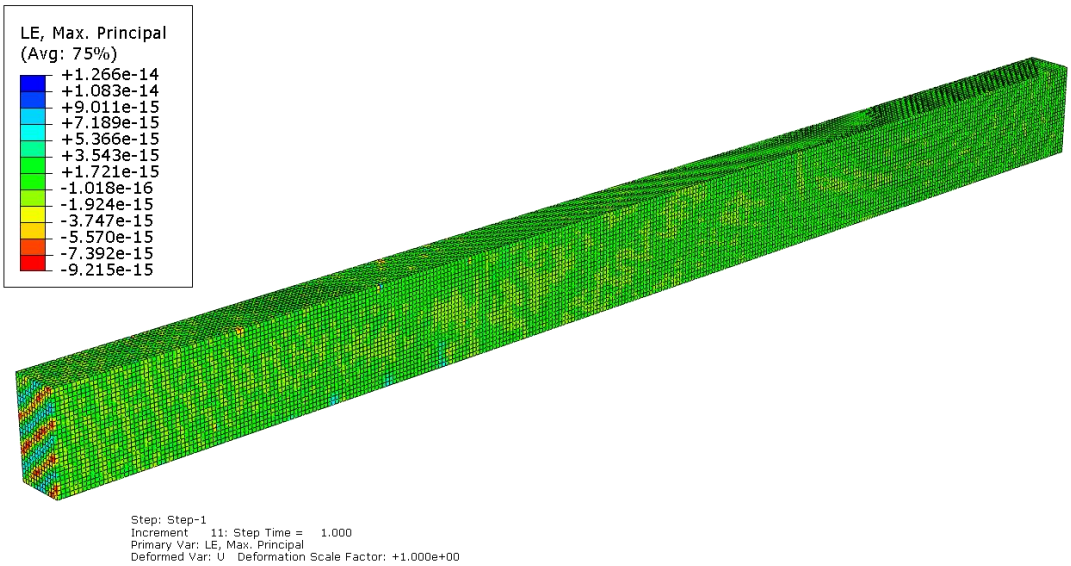

Figure 10: Logarithmic strain contours of the entire outer surface of the beam

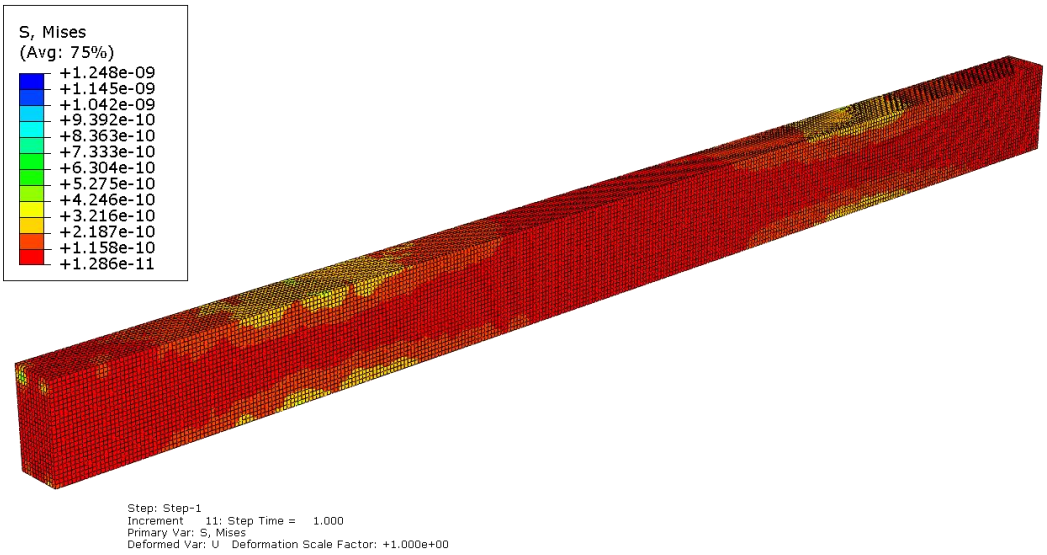

Figure 11: Von-Mises stress contours of the beam's outer surface

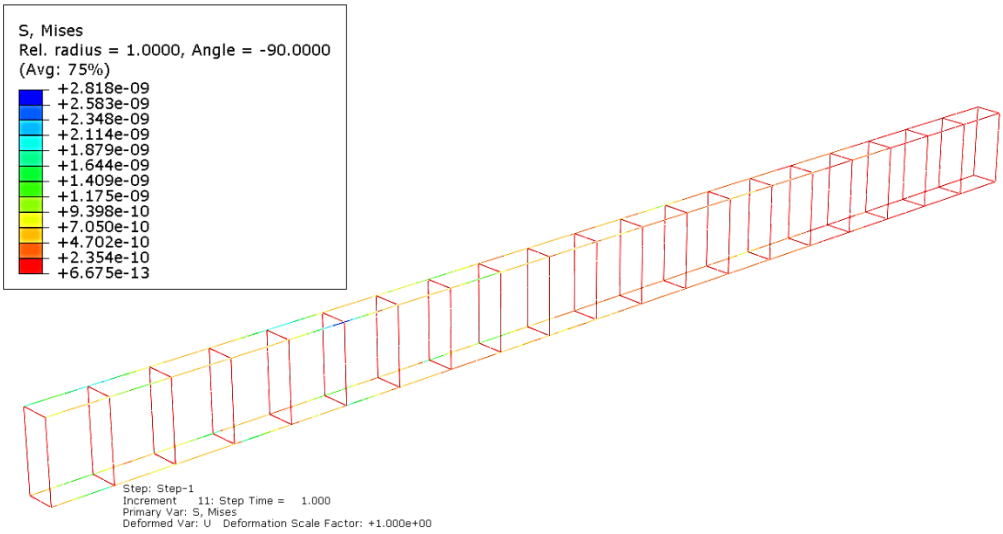

Figure 12: Von-Mises stress contours of the beam reinforcement

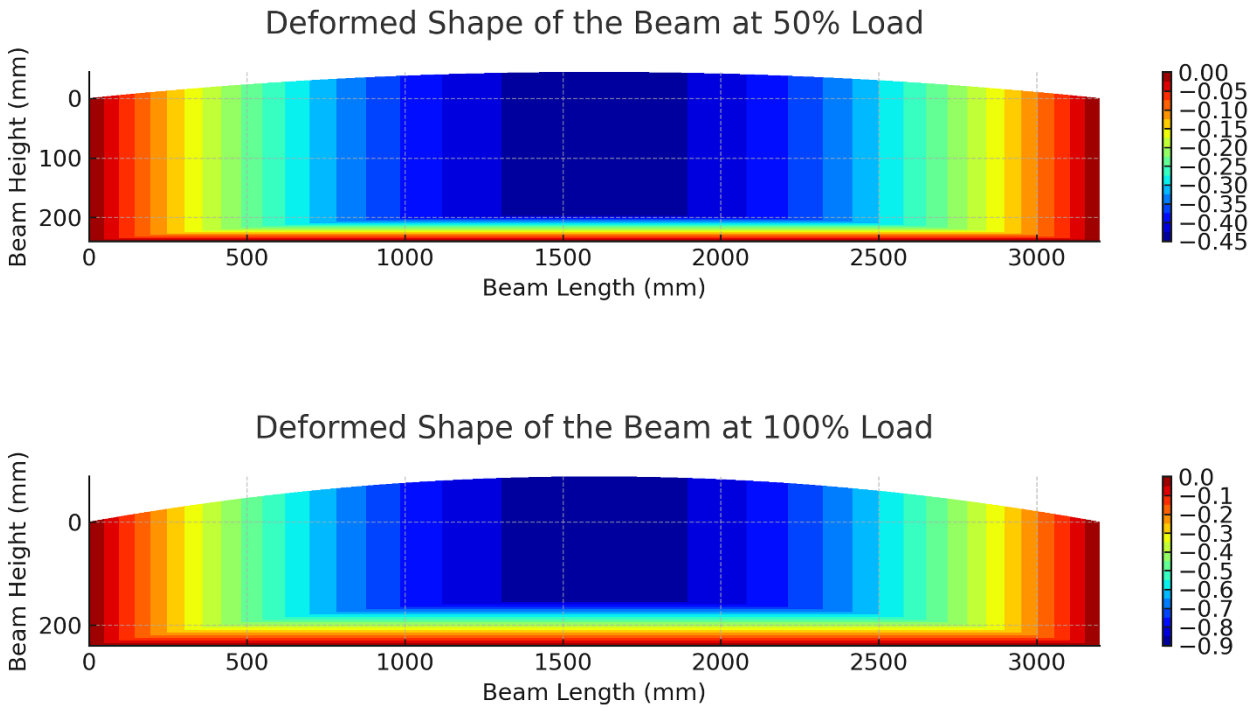

Figure 13: Deformed shape of the beam at 50% and 100% load (failure stage) with vertical displacement (mm) contours

3.5 Comparison between Analytical, Experimental and Numerical Data

To assess the time-dependent deflection of UHPFRC beams, this study incorporates the proposed creep coefficient formula, shrinkage strain formula, aging coefficient, and shrinkage-induced curvature factor into the theoretical framework outlined in ACI Committee 435-R95 (2003). These parameters were used to compute theoretical time-dependent deflection based on the applied service loads, including the self-weight of the beam. The deflection was analyzed through three approaches: analytical prediction, numerical simulation using ABAQUS, and experimental measurements, as reported by Bărbos (2016). The time-dependent deflection was first computed analytically, employing the proposed formulations to account for the long-term effects of creep and shrinkage on beam deflection. Additionally, the deflection was assessed numerically in ABAQUS by simulating the beam's behavior over time under sustained loading conditions. Experimental deflection results from Bărbos (2016) were then compared against analytical and numerical outcomes to validate the proposed analytical model and the numerical simulations.

Figure 14 compares analytical predictions, numerical results, and experimental deflection data for UHPFRC beams with varying steel fiber ratios. A close fit is observed between the analytical predictions and experimental results, particularly for the control beam with no added fibers. The analytical model performs well initially but exhibits slight overestimation after 28 days, which persists until the beam stabilizes. This discrepancy can be attributed to inelastic behaviors in the beam that are not fully captured by the elastic assumptions in the analytical model. Despite this, the analytical approach provides a conservative deflection estimate, with an average deviation of approximately 20% from experimental values. Studies by (Tan & Saha, 2005) and Ashour et al. (2000) indicated that deflection was reduced by 26% and 34% when steel fiber content was increased by 1.5% and 2%, respectively, compared to a control specimen without fibers. Similarly, the analytical approach in this research aligns with these findings, showing a 32% reduction in deflection with a 1.5% steel fiber addition and a 40% reduction with a 2.55% steel fiber addition relative to the control beam. This confirms the beneficial effect of fiber reinforcement on deflection performance, as observed in both experimental and analytical predictions.

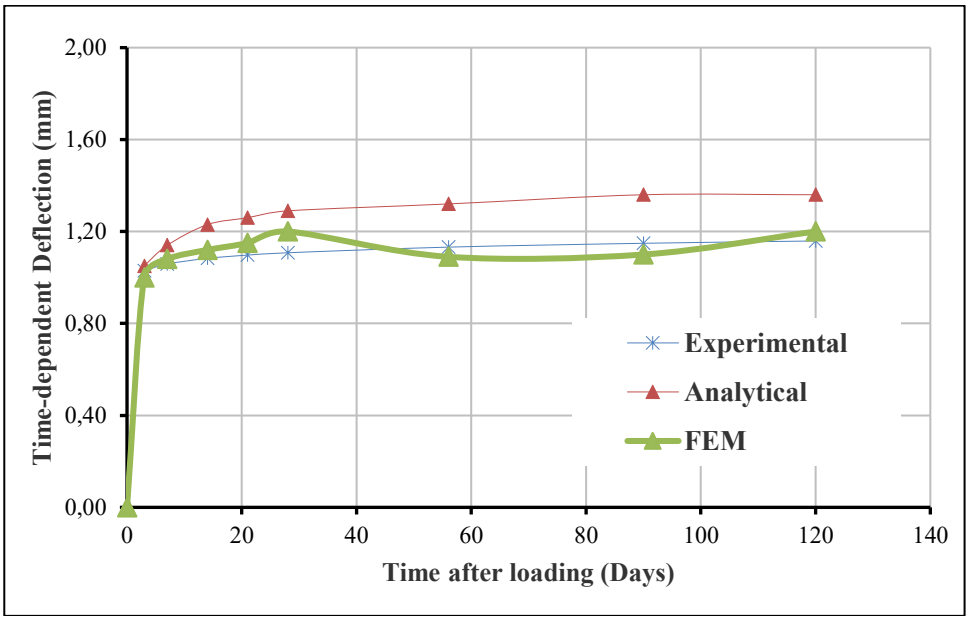
2,00
1,60
1,20
0,80
0,40
0,00
Time-dependent Deflection (mm)
0
20
40
60
80
100
120
140
Time after loading (Days)
Experimental
Analytical
FEM

(a)

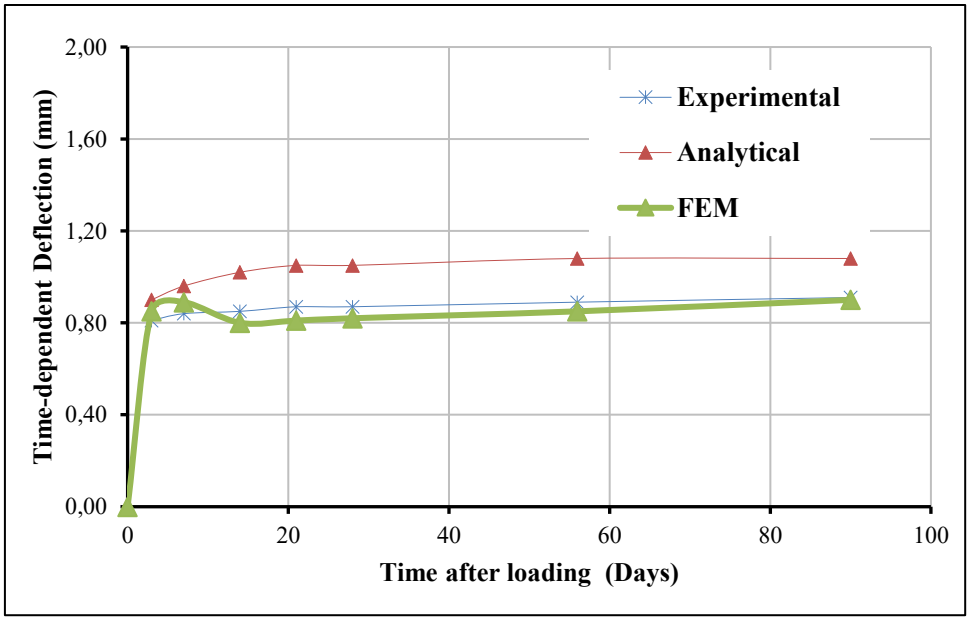
2,00
1,60
1,20
0,80
0,40
0,00
Time-dependent Deflection (mm)
0
20
40
60
80
100
Time after loading (Days)
Experimental
Analytical
FEM

(b)

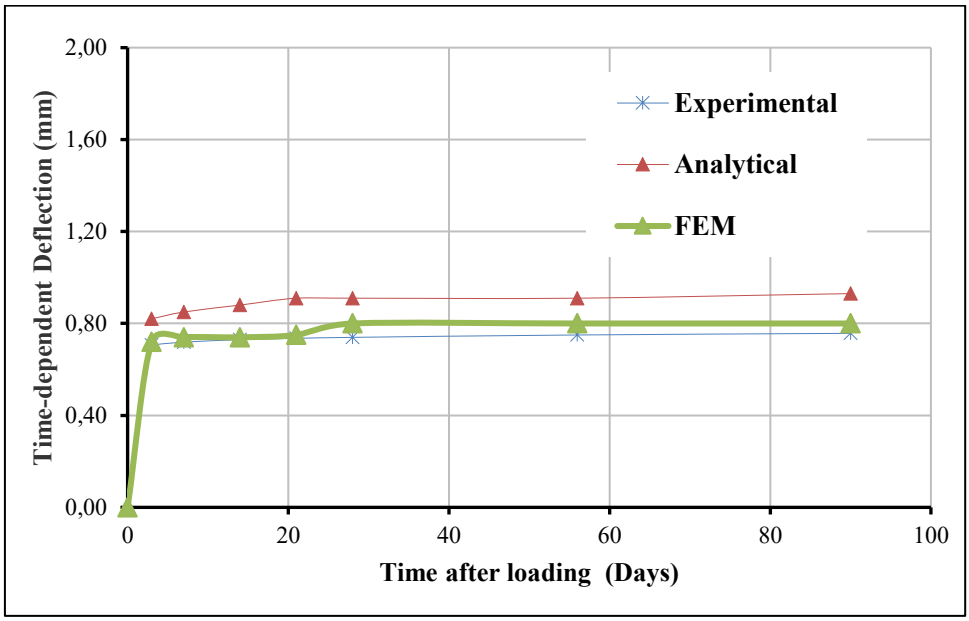

(c)

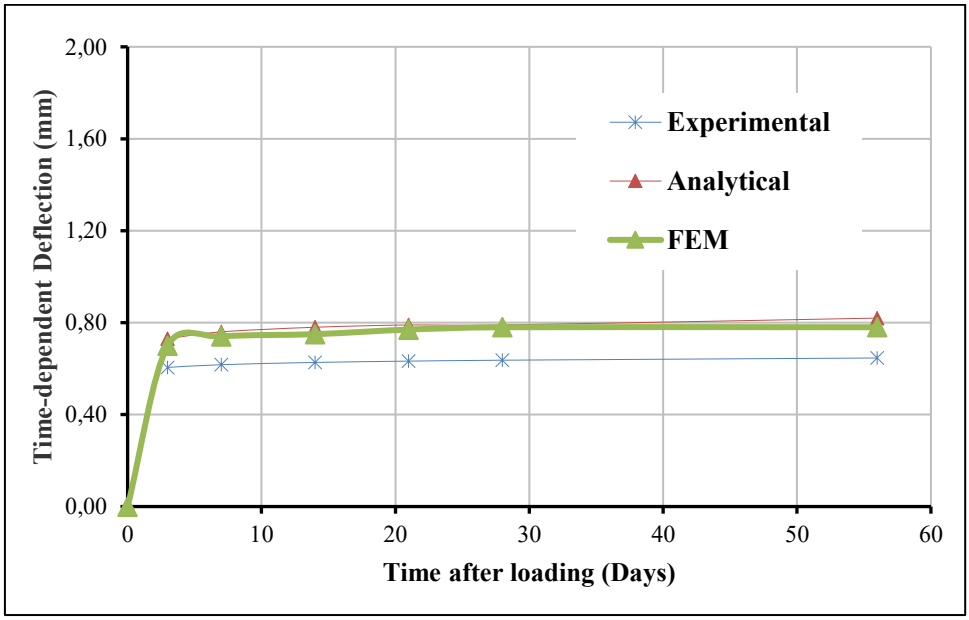

(d)

Figure 14: Analytical and experimental deflection comparison: (a) 0% steel fiber, (b) 0.5% steel fiber, (c) 1.5% steel fiber, and (d) 2.55% steel fiber

A detailed statistical analysis was carried out based on analytical and experimental deflection values to evaluate the consistency in mean values across the experiment, model, and FEM analyses. Table 4 presents the statistical comparison between experimental and analytical deflection values for UHPFRC beams with varying steel fiber content (0%, 0.5%, 1.5%, and 2.55%). The findings illustrate a robust consistency in mean deflection values across the experimental, model, and FEM analyses, with standard errors remaining below 0.05, signifying high reliability in the measurements. The slight variation in median and mode values reflects the inherent differences in data distribution between experimental and analytical approaches. Notably, the standard deviation and sample variance values align closely among the methods, emphasizing the uniformity of the results. Additionally, the negative kurtosis and positive skewness observed across the datasets indicate a slight deviation from normality, likely influenced by the controlled experimental conditions and the

unique material properties of UHPFRC. These results underscore the accuracy and validity of the analytical models in predicting deflection behavior, providing confidence in their applicability for design and analysis purposes.

Table 4 Statistical analyses for analytical and experimental deflection comparison: (a) 0% steel fiber (b) 0.5% steel fiber (c) 1.5% steel fiber (d) 2.55% steel fiber

Experiment		*Model*		*FEM*	
Mean	0.85	Mean	1.00	Mean	0.88
Standard Error	0.04	Standard Error	0.04	Standard Error	0.03
Median	0.83	Median	0.95	Median	0.81
Mode	0.87	Mode	1.05	Mode	0.80
Standard Deviation	0.19	Standard Deviation	0.19	Standard Deviation	0.16
Sample Variance	0.03	Sample Variance	0.04	Sample Variance	0.03
Kurtosis	-1.22	Kurtosis	-0.86	Kurtosis	-0.73
Skewness	0.41	Skewness	0.54	Skewness	0.89
Range	0.55	Range	0.63	Range	0.50
Minimum	0.61	Minimum	0.73	Minimum	0.70
Maximum	1.16	Maximum	1.36	Maximum	1.20
Confidence Level (95.0%)	0.07	Confidence Level (95.0%)	0.08	Confidence Level (95.0%)	0.06

4 Conclusions

In this study, the time-dependent deflection of UHPFRC beams was predicted both analytically and numerically using FEM and compared with experimental results. Based on the research findings, the following conclusions are drawn:

- In the analytical modeling of the time-dependent deflection of UHPFRC beams, the creep coefficient and shrinkage strain are two essential parameters. It was found that the present formulation for the creep coefficient and shrinkage strain can estimate the time-dependent experimental values with sufficient accuracy. At early stages, the present formulation can efficiently predict the experimental values while slightly underestimating the actual values at later times, indicating the efficiency of the formulation.
- The time-dependent deflection of UHPFRC beams with varying percentages of fiber under different sustained loads was predicted in the present study. It was found that both the total and time-dependent deflections decrease with the increase in fiber reinforcement percentage in the UHPFRC beams. However, the beam experiences higher deflection at higher sustained loads, which is expected. Moreover, the control beam (0% steel fiber) shows a linear relationship between time and deflection throughout the entire service period of the beam. In contrast, the deflection increases with time and is relatively insignificant beyond 28 days up to the stabilization period for all the beams with steel fiber, which indicates the beneficial effect of fiber reinforcement in UHPFRC beams against time-dependent deflection.
- The regression and ANOVA analyses were carried out on the predicted analytical results, and they indicated that the overall deflection behavior of the UHPFRC beam has a strong dependency on time-dependent effects, particularly at higher loads, indicating the importance of incorporating time-dependent parameters in the analysis of UHPFRC beams under sustained loading conditions.
- Based on the comparison between analytical, finite element method (FEM), and experimental results, the proposed model was found to provide a conservative estimate of experimental deflections, with an average deviation of approximately 20%. In the early stages (within the first 7 days), both the analytical and FEM models were able to predict time-dependent deflection with reasonable accuracy. The analytical model generally overestimated deflections, while the FEM model tended to underestimate them. Notably, the deviation between experimental and predicted values decreased with higher percentages of steel fiber. However, statistical analysis demonstrated strong consistency in the mean deflection values across experimental, analytical, and FEM approaches, with standard errors remaining below 0.05. This indicates the reliability and accuracy of the proposed analytical model in predicting deflection behavior.

Acknowledgment

The overall data analysis and modeling for this research work were carried out with the high-speed computer in the BIM laboratory of the Department of Building Engineering and Construction Management, Khulna University of Engineering and Technology, Khulna-9203, Bangladesh. The author would like to express gratitude to the laboratory assistant of the BIM laboratory and other associated persons for providing their support, knowledge, and valuable time during this research.

Editor: Marco L. Bittencourt

References

Abbas, S., Nehdi, M., & Saleem, M. (2016). Ultra-high performance concrete: Mechanical performance, durability, sustainability and implementation challenges. *International Journal of Concrete Structures and Materials*, *10*(3), 271-295.

ACI Committee 435R-95. (2003). *Control of deflection in concrete structures*.

Ahmed, E., & Sobuz, H. R. . (2011). Experimental study on long-term behaviour of CFRP strengthened RC beams under sustained load. *Structural engineering and mechanics: An international journal*, *40*(1), 105-120.

Ahmed, E., & Sobuz, H. R. (2011a). Flexural and time-dependent performance of palm shell aggregate concrete beam. *KSCE Journal of Civil Engineering*, *15*(5), 859-865. https://doi.org/10.1007/s12205-011-1148-2

Ahmed, E., & Sobuz, H. R. (2011b). Immediate and Long-Term Deflection of Carbon Fiber Reinforced Polymer (CFRP) Concrete Beams. *Key Engineering Materials*, *471-472*, 73-78. https://doi.org/10.4028/www.scientific.net/KEM.471-472.73

Ahmed, E., Sobuz, H. R., & Sutan, N. M. (2011). Flexural performance of CFRP strengthened RC beams with different degrees of strengthening schemes *International Journal of the Physical Sciences*, *6*(9), 2229-2238.

Akhnoukh, A. K., & Buckhalter, C. (2021). Ultra-high-performance concrete: Constituents, mechanical properties, applications and current challenges. *Case Studies in Construction Materials*, *15*, e00559.

Akid, A. S. M., Shah, S. M. A., Sobuz, M. D. H. R., Tam, V. W. Y., & Anik, S. H. (2021). Combined influence of waste steel fibre and fly ash on rheological and mechanical performance of fibre-reinforced concrete. *Australian Journal of Civil Engineering*, *19*(2), 208-224. https://doi.org/10.1080/14488353.2020.1857927

Akid, A. S. M., Wasiew, Q. A., Sobuz, M. H. R., Rahman, T., & Tam, V. W. (2021). Flexural behavior of corroded reinforced concrete beam strengthened with jute fiber reinforced polymer. *Advances in Structural Engineering*, *24*(7), 1269-1282. https://doi.org/10.1177/1369433220974783

Ashour, S., Mahmood, K., Wafa, F., & Associate. (2000). Service Load Deflections of High-Strength Fiber Service Load Deflections of High-Strength Fiber Reinforced Concrete Beams. *Journal of King Abdulaziz University-Engineering Sciences*, *12*. https://doi.org/10.4197/Eng.12-2.2

Bărbos, G. A. (2016). Long-term behavior of ultra–high performance concrete (UHPC) bended beams. *Procedia Technology*, *22*, 203-210.

Branson, D. E. (1977). *Deformation of Concrete Structures*. McGraw Hill Book Co., Advanced Book Program.

BS 8110-1. (1997). *Structural use of concrete-Part 1: Code of practice for design and Construction British Standard*.

Chen, D., Chen, Y., Ma, L., Sobuz, M. H. R., Kabbo, M. K. I., & Khan, M. M. H. (2024). A state of review on manufacturing and effectiveness of ultra-high-performance fiber reinforced concrete for long-term integrity of concrete structures. *Advances in concrete construction*, *17*(5), 293-310.

Das, S., Habibur Rahman Sobuz, M., Tam, V. W. Y., Akid, A. S. M., Sutan, N. M., & Rahman, F. M. M. (2020). Effects of incorporating hybrid fibres on rheological and mechanical properties of fibre reinforced concrete. *Construction and Building Materials*, *262*, 120561. https://doi.org/https://doi.org/10.1016/j.conbuildmat.2020.120561

Ebadi Jamkhaneh, M., & Kafi, M. A. (2018). Equalizing octagonal PEC columns with steel columns: Experimental and theoretical study. *Practice Periodical on Structural Design and Construction*, *23*(3), 04018012.

El-Din, H. K. S., Mohamed, H. A., Khater, M. A. E.-H., & Ahmed, S. (2016). Effect of steel fibers on behavior of ultra high performance concrete. International Interactive Symposium on Ultra-High Performance Concrete,

F. F. Al-Ajmai, F. A. A.-O., and H. M. Aldaihani. (2018). Effect of type of ground cover on the ground cooling potential for buildings in extreme desert climate. *Jordan Journal of Civil Engineering*, *12*(3).

Flietstra, J., Ahlborn, T. M., Harris, D. K., & De Melo e Silva, H. (2012). Creep behaviour of UHPC under compressive loading with varying curing regimes. 3rd International Symposium on UHPC, Kassel, Germany,

Ghasemi, M., Zhang, C., Khorshidi, H., Zhu, L., & Hsiao, P.-C. (2023). Seismic upgrading of existing RC frames with displacement-restraint cable bracing. *Engineering Structures*, *282*, 115764. https://doi.org/https://doi.org/10.1016/j.engstruct.2023.115764

Gilbert, I. (2001). Shrinkage, cracking and deflection-the serviceability of concrete structures. *Electronic Journal of Structural Engineering*, *1*(1), 15-37.

Graybeal, B. A. (2006). *Material property characterization of ultra-high performance concrete*.

Graybeal, B. A., & Stone, B. (2012). *Compression response of a rapid-strengthening ultra-high performance concrete formulation*.

Habibur Rahman Sobuz, M., Khan, M. H., Kawsarul Islam Kabbo, M., Alhamami, A. H., Aditto, F. S., Saziduzzaman Sajib, M., Johnson Alengaram, U., Mansour, W., Hasan, N. M. S., Datta, S. D., & Alam, A. (2024). Assessment of mechanical properties with machine learning modeling and durability, and microstructural characteristics of a biochar-cement mortar composite. *Construction and Building Materials*, *411*, 134281. https://doi.org/https://doi.org/10.1016/j.conbuildmat.2023.134281

Hasan, N. M. S., Visintin, P., Oehlers, D. J., Bennett, T., & Sobuz, M. H. R. (2019). Time dependent deflection of RC beams allowing for partial interaction and non-linear shrinkage. *Materials and Structures*, *52*(3), 52. https://doi.org/10.1617/s11527-019-1350-0

Hasan, R., Sobuz, M. H. R., Akid, A. S. M., Awall, M. R., Houda, M., Saha, A., Meraz, M. M., Islam, M. S., & Sutan, N. M. (2023). Eco-friendly self-consolidating concrete production with reinforcing jute fiber. *Journal of Building Engineering*, *63*, 105519. https://doi.org/https://doi.org/10.1016/j.jobe.2022.105519

Hossain, M. A., Datta, S. D., Akid, A. S. M., Sobuz, M. H. R., & Islam, M. S. (2023). Exploring the synergistic effect of fly ash and jute fiber on the fresh, mechanical and non-destructive characteristics of sustainable concrete. *Heliyon*, *9*(11), e21708. https://doi.org/https://doi.org/10.1016/j.heliyon.2023.e21708

Huang, H., Huang, M., Zhang, W., & Yang, S. (2021). Experimental study of predamaged columns strengthened by HPFL and BSP under combined load cases. *Structure and Infrastructure Engineering*, *17*(9), 1210-1227. https://doi.org/10.1080/15732479.2020.1801768

Jabin, J. A., Khondoker, M. T. H., Sobuz, M. H. R., & Aditto, F. S. (2024). High-temperature effect on the mechanical behavior of recycled fiber-reinforced concrete containing volcanic pumice powder: An experimental assessment combined with machine learning (ML)-based prediction. *Construction and Building Materials*, *418*, 135362. https://doi.org/https://doi.org/10.1016/j.conbuildmat.2024.135362

Kang, S.-T., Lee, Y., Park, Y.-D., & Kim, J.-K. (2010). Tensile fracture properties of an Ultra High Performance Fiber Reinforced Concrete (UHPFRC) with steel fiber. *Composite structures*, *92*(1), 61-71.

Khan, M. M. H., Sobuz, M. H. R., Meraz, M. M., Tam, V. W. Y., Hasan, N. M. S., & Shaurdho, N. M. N. (2023). Effect of various powder content on the properties of sustainable self-compacting concrete. *Case Studies in Construction Materials*, *19*, e02274. https://doi.org/https://doi.org/10.1016/j.cscm.2023.e02274

Khazanovich, L. (1990). Age-adjusted effective modulus method for time-dependent loads. *Journal of engineering mechanics*, *116*(12), 2784-2789.

Kilpatrick, A. E., & Gilbert, R. I. (2018). Simplified calculation of the long-term deflection of reinforced concrete flexural members. *Australian Journal of Structural Engineering*, *19*(1), 34-43. https://doi.org/10.1080/13287982.2017.1368071

Liu, H., Zhang, B., Yan, L., Meng, X., Zhou, J., Cui, J., & Spencer, B. F. (2025). Rebar characterization using dual-polarization GPR. *NDT & E International*, *154*, 103391. https://doi.org/https://doi.org/10.1016/j.ndteint.2025.103391

Long, X., Mao, M.-h., Su, T.-x., Su, Y.-t., & Tian, M.-k. (2023). Machine learning method to predict dynamic compressive response of concrete-like material at high strain rates. *Defence Technology*, *23*, 100-111. https://doi.org/https://doi.org/10.1016/j.dt.2022.02.003

Md. Sadiqul Hasan, N., Rahman Sobuz, H., Sharif Auwalu, A., & Tamanna, N. (2015). Investigation Into The Suitability Of Kenaf Fiber To Produce Structural Concrete. *Advanced Materials Letters*, *6*(8), 731-737. https://doi.org/10.5185/amlett.2015.5818

Miah, M. J., Miah, M. S., Hasan, N. M. S., Sobuz, M. H. R., & Li, Y. (2025). Role of recycled crushed clay bricks as fine aggregates in enhancing the performance of ferrocement-strengthened RC beams. *Construction and Building Materials*, *478*, 141412. https://doi.org/https://doi.org/10.1016/j.conbuildmat.2025.141412

Mishra, M. (2024). Quantifying compressive strength in limestone powder incorporated concrete with incorporating various machine learning algorithms with SHAP analysis. *Asian Journal of Civil Engineering*. https://doi.org/10.1007/s42107-024-01219-1

Mishra, M., Das, D., Laurinavicius, A., Laurinavicius, A., & Chang, B. H. (2025). Sectorial Analysis of Foreign Direct Investment and Trade Openness on Carbon Emissions: A Threshold Regression Approach. *Journal of International Commerce, Economics and Policy*, *16*(01), 2550003. https://doi.org/10.1142/s1793993325500036

Niu, Y., Wang, W., Su, Y., Jia, F., & Long, X. (2024). Plastic damage prediction of concrete under compression based on deep learning. *Acta Mechanica*, *235*(1), 255-266. https://doi.org/10.1007/s00707-023-03743-8

Perry, V., & Zakariasen, D. (2004). First use of ultra-high performance concrete for an innovative train station canopy. *Concrete Technology Today*, *25*(2), 1-2.

Rahman Sobuz, M. H., Alam, A., John Oehlers, D., Visintin, P., Hamid Sheikh, A., Mohamed Ali, M. S., & Griffith, M. (2023). Experimental and analytical studies of size effects on compressive ductility response of Ultra-High-Performance Fiber-Reinforced concrete. *Construction and Building Materials*, *409*, 133864. https://doi.org/https://doi.org/10.1016/j.conbuildmat.2023.133864

Resplendino, J. (2012). State of the art of design and construction of UHPFRC structures in France. Proceedings of Hipermat-3rd International Symposium on UHPC and Nanotechnology for Construction Materials,

Russell, H. G., Graybeal, B. A., & Russell, H. G. (2013). *Ultra-high performance concrete: A state-of-the-art report for the bridge community*.

Sayed Mohammad Akid, A., Hossain, S., Imtiaz Uddin Munshi, M., Elahi, M. M. A., Habibur Rahman Sobuz, M., Tam, V. W. Y., & Saiful Islam, M. (2023). Assessing the influence of fly ash and polypropylene fiber on fresh, mechanical and durability properties of concrete. *Journal of King Saud University - Engineering Sciences*, *35*(7), 474-484. https://doi.org/https://doi.org/10.1016/j.jksues.2021.06.005

Shi, T., Li, K.-M., Wang, C.-Z., Jin, Z., Hao, X.-K., Sun, P., Han, Y.-X., Pan, C.-G., Fu, N., & Wang, H.-B. (2025). Fracture toughness of recycled carbon fibers reinforced cement mortar and its environmental impact assessment. *Case Studies in Construction Materials*, *22*, e04866. https://doi.org/https://doi.org/10.1016/j.cscm.2025.e04866

Sobuz, H., Visintin, P., Ali, M. M., Singh, M., Griffith, M., & Sheikh, A. (2016). Manufacturing ultra-high performance concrete utilising conventional materials and production methods. *Construction and Building materials*, *111*, 251-261.

Sobuz, H. R., & Ahmed, E. (2011). Flexural Performance of RC Beams Strengthened with Different Reinforcement Ratios of CFRP Laminates. *Key Engineering Materials*, *471-472*, 79-84. https://doi.org/10.4028/www.scientific.net/KEM.471-472.79

Sobuz, H. R., Ahmed, E., & Sutan, N. M. (2011). Deflection and cracking behavior of RC beams externally reinforced with carbon fiber laminates. *Journal of Reinforced Plastics and Composites*, *30*(21), 1807-1818. https://doi.org/10.1177/0731684411419908

Sobuz, H. R., Ahmed, E., Sutan, N. M., Hasan, N. M. S., Uddin, M. A., & Uddin, M. J. (2012). Bending and time-dependent responses of RC beams strengthened with bonded carbon fiber composite laminates. *Construction and Building materials*, *29*, 597-611.

Sobuz, H. R., Ahmed, E., Sutan, N. M., Sadiqul Hasan, N. M., Alhaz Uddin, M., & Jahir Uddin, M. (2012). Bending and time-dependent responses of RC beams strengthened with bonded carbon fiber composite laminates. *Construction and Building Materials*, *29*, 597-611. https://doi.org/https://doi.org/10.1016/j.conbuildmat.2011.11.006

Sobuz, H. R., Oehlers, D. J., Visintin, P., Hasan, N. M. S., Hoque, M. I., & Akid, A. S. M. . (2017). Flow and strength characteristics of ultra-high performance fiber reinforced concrete: Influence of fiber type and volume-fraction. *Journal of Civil Engineering and Construction*, *6*(1), 15-21.

Sobuz, M. H. R., Islam, M. S., Akid, A. S. M., Datta, S. D., Alahmari, T. S., Hasan, N. M. S., Khondoker, M. T. H., & Aditto, F. S. (2023). Mechanical Properties and Flexural Response of Palm Shell Aggregate Lightweight Reinforced Concrete Beam. *Sustainability*, *15*(22), 15783. https://www.mdpi.com/2071-1050/15/22/15783

Sobuz, M. H. R., Kabbo, M. K. I., Alahmari, T. S., Ashraf, J., Gorgun, E., & Khan, M. M. H. (2025). Microstructural behavior and explainable machine learning aided mechanical strength prediction and optimization of recycled glass-based solid waste concrete. *Case Studies in Construction Materials*, *22*, e04305. https://doi.org/https://doi.org/10.1016/j.cscm.2025.e04305

Sobuz, M. H. R., Khan, M. H., Islam, M. R., Kabbo, M. K. I., Alzlfawi, A., Jameel, M., & Khan, M. M. H. (2025). Combined influence of crushed brick powder and recycled concrete aggregate on the mechanical, durability and microstructural properties of eco-concrete: An experimental and machine learning-based evaluation. *Journal of Materials Research and Technology*, *36*, 8757-8776. https://doi.org/https://doi.org/10.1016/j.jmrt.2025.05.118

Sobuz, M. H. R., Rahman, M. M., Aayaz, R., Al-Rashed, W. S., Datta, S. D., Safayet, M. A., Kabbo, M. K. I., & Abdullah, M. (2025). Combined influence of modified recycled concrete aggregate and metakaolin on high-strength concrete production: Experimental assessment and machine learning quantifications with advanced SHAP and PDP

analyses. *Construction and Building Materials*, *461*, 139897. https://doi.org/https://doi.org/10.1016/j.conbuildmat.2025.139897

Sun, G., Kong, G., Liu, H., & Amenuvor, A. C. (2017). Vibration velocity of X-section cast-in-place concrete (XCC) pile–raft foundation model for a ballastless track. *Canadian Geotechnical Journal*, *54*(9), 1340-1345. https://doi.org/10.1139/cgj-2015-0623

Tan, K. H., & Saha, M. K. (2005). Ten-year study on steel fiber-reinforced concrete beams under sustained loads. *ACI Structural Journal,*, *102*(3), 472.

Tan, K. H., & Saha, M. K. (2006). Long-term deflections of reinforced concrete beams externally bonded with FRP system. *Journal of Composites for Construction*, *10*(6), 474-482.

Wu, Z., Shi, C., & Khayat, K. H. (2019). Investigation of mechanical properties and shrinkage of ultra-high performance concrete: Influence of steel fiber content and shape. *Composites Part B: Engineering*, *174*, 107021.

Xu, Y., Liu, J., Liu, J., Zhang, P., Zhang, Q., & Jiang, L. (2018). Experimental studies and modeling of creep of UHPC. *Construction and Building materials*, *175*, 643-652.

Yang, C., Nan, Z., Huo, Y., Yang, Y., Xu, P., Xiao, Y., Fang, Y., & Meng, K. (2025). Design, characterisation, and crushing performance of hexagonal-quadrilateral lattice-filled steel/CFRP hybrid structures. *Composites Part B: Engineering*, *304*, 112631. https://doi.org/https://doi.org/10.1016/j.compositesb.2025.112631

Yang, G., Zhao, H., Hu, Z., Zhang, W., Xiang, Y., Jin, M., Wan-Wendner, R., & Liu, J. (2025). Prediction of restrained stress for UHPC: Considering relationship between long-term and in-situ creep. *Construction and Building materials*, *484*, 141722. https://doi.org/https://doi.org/10.1016/j.conbuildmat.2025.141722

Yao, S., Chen, F., Wang, Y., Zhou, H., & Liu, K. (2025). Manufacturing defect-induced multiscale weakening mechanisms in carbon fiber reinforced polymers captured by 3D CT-based machine learning and high-fidelity modeling. *Composites Part A: Applied Science and Manufacturing*, *197*, 109052. https://doi.org/https://doi.org/10.1016/j.compositesa.2025.109052

Yao, Y., Huang, H., Zhang, W., Ye, Y., Xin, L., & Liu, Y. (2022). Seismic performance of steel-PEC spliced frame beam. *Journal of Constructional Steel Research*, *197*, 107456. https://doi.org/https://doi.org/10.1016/j.jcsr.2022.107456

Yao, Y., Zhou, L., Huang, H., Chen, Z., & Ye, Y. (2023). Cyclic performance of novel composite beam-to-column connections with reduced beam section fuse elements. *Structures*, *50*, 842-858. https://doi.org/https://doi.org/10.1016/j.istruc.2023.02.054

Yoo, D.-Y., Kim, S., & Kim, M.-J. (2018). Comparative shrinkage behavior of ultra-high-performance fiber-reinforced concrete under ambient and heat curing conditions. *Construction and Building materials*, *162*, 406-419.

Zhai, Z., Shu, Q., Chen, H., & Liu, Y. (2025). CCQC-based multi-seismic level optimum design of supplemental dampers in steel moment resisting frame. *Journal of Building Engineering*, *108*, 112922. https://doi.org/https://doi.org/10.1016/j.jobe.2025.112922

Zhang, W., Yang, X., Lin, J., Lin, B., & Huang, Y. (2024). Experimental and numerical study on the torsional behavior of rectangular hollow reinforced concrete columns strengthened By CFRP. *Structures*, *70*, 107690. https://doi.org/https://doi.org/10.1016/j.istruc.2024.107690

Zhu, L., Wang, J.-J., Li, X., Zhao, G.-Y., & Huo, X.-J. (2020). Experimental and numerical study on creep and shrinkage effects of ultra high-performance concrete beam. *Composites Part B: Engineering*, *184*, 107713.

Zvolánek, L., & Terzijski, I. (2017). Relaxation of Structural Concrete due to its Shrinkage in Terms of Age-Adjusted Effective Modulus Method. *Key Engineering Materials*, *737*, 471-476. https://doi.org/10.4028/www.scientific.net/KEM.737.471